communications physics

Article

https://doi.org/10.1038/s42005-024-01633-6

Collimated muon beam proposal for probing neutrino charge-parity violation

Check for updates

Alim Ruzi ✉, Tianyi Yang, Dawei Fu, Sitian Qian, Leyun Gao & Qiang Li ✉

The phenomenon of neutrino oscillation is of great theoretical and experimental interest for our understand of the nature of the neutrino and its implication for physics beyond the standard Model. Currently available neutrino oscillation experiments can already constrain neutrino mixing parameters with a confidence level up to 3 standard deviations (σ). However, it remains challenging to provide a deterministic constraint on the Charge-Parity (CP) violation phase of the neutrino mixing matrix. Here, we propose an experimental setup that exploits collimated muon beams to probe neutrino CP-violation. In our proposed acceleration experiment, a 45 GeV positron source with additional muon collimation, interfaces with near-future neutrino detectors like DUNE and T2K, to probe neutrino CP-violation phase with a significantly higher sensitivity than obtained with the neutrino detectors alone, and to determine tau neutrino properties. Simulations estimate the collection of 10^4 tau (anti-) neutrino in 5 years, and a sensitivity of over 7 standard deviations for $\delta_{CP} = |\pi/2|$ in 5 years. Collecting ν_τ appearance events from μ^- and μ^+ beams over 10 years can attain a 3-4 standard deviation sensitivity. This proposal may serve as a tau factory.

Neutrinos are among the most abundant and least understood of all particles that make up our universe. Neutrino physics has made significant progress in the past few decades. One of the major discovery is the observation of neutrino oscillations[1–3], confirming that at least two types of Standard Model (SM) neutrinos have a small, but strictly nonzero mass. Neutrino oscillations also solved the mysterious solar and atmospheric neutrino problem[4–8]. The neutrino oscillations in the presence of three active neutrino flavors are described by the mass square differences i.e., $\Delta m^2_{21} = m^2_2 - m^2_1, \Delta m^2_{31} = m^2_3 - m^2_1$, three mixing angles, θ_{12}, θ_{23}, and θ_{13}, and one Dirac phase, δ_{CP}. There are another two parameters: the Majorana phases, δ_1, δ_2, which play a part in the neutrinoless double beta decay[9] and are directly related to the nature of the neutrino. The mixing angles and the phases are the elements of a unitary matrix called Pontecorvo–Maki–Nakagawa–Sakata (PMNS) matrix[10,11]. The available experiments on neutrino oscillations to date have measured five of the neutrino mixing parameters, three mixing angles θ_{12}, θ_{13}, θ_{23}, and the two squared-mass differences Δm^2_{21}, $|\Delta m^2_{32}|$ up to 3σ confidence level[12–16]. Among these parameters, the sign of atmospheric mass-squared difference, i.e., Δm_{31}, which will determine the mass ordering problem, the octant of the mixing angle θ_{23}, and the the true value of the CP-violating phase δ_{CP} remain unknown. The determination of the CP-violating phase, the Dirac phase, has been the core research program in neutrino physics for years because it provides a potential source of CP violation in the SM lepton sector. It has been known that the leptonic CP violation could generate the matter–antimatter asymmetry through leptogenesis[17]. CP violation in neutrino oscillation can be measured through the difference between the oscillation probability of the neutrino and antineutrino, expressed as $\Delta P^{CP}_{\alpha\beta} = P_{\alpha\beta} - \overline{P}_{\alpha\beta}$, which is well quantified by δ_{CP}. There are several experiments worldwide dedicated to the measurements of the neutrino parameters, especially the CP phase, performing searches of short-baseline and long-baseline neutrino oscillation.

To ensure that there are enough neutrino flavors oscillated from high-energy neutrinos, a long-baseline neutrino oscillation experiment is preferable rather than a short baseline. The long-baseline experiments, T2K (Tokai to Kamioka)[14,18–21] and NOvA[22] have recently reported their results. T2K reports a measured value for the CP phase, $\delta_{CP} = -1.97^{+0.97}_{-0.70}$ while excluding $\delta_{CP} = 0$ and π at 90% CL, indicating CP violation in the lepton sector at relatively improved confidence level. However, there is CP-conserving values for δ_{CP} within 3σ standard error[21]. The far detector in this case is the Super-Kamiokande, a 50 Kton water Cherenkov detector. A narrow band neutrino beam is produced at an angle of 2. 5° by a 30 GeV proton beam hitting on graphite target. With this off-axis method, the narrow band neutrino energy has a peak at 0.6 GeV. The secondary neutrino produced from decays of Kaon or Pion travels a distance of 295 Km to reach the Super-Kamiokande detector. T2K plans to extend its term to 2026, followed by the Hyper-K project[23] with the mass of the far detector to be increased by a factor of 10, and will offer a broad science program. The NOvA experiment[22] is also a

State Key Laboratory of Nuclear Physics and Technology, School of Physics, Peking University, Beijing, China. ✉e-mail: alim.ruzi@pku.edu.cn; qliphy0@pku.edu.cn

long-baseline accelerator-based neutrino oscillation experiment. It uses the upgraded Fermilab NuMI beam and measures electron neutrino appearance and muon neutrino disappearance at its far detector in Ash River, Minnesota. The reported NOvA result shows no strong preference for any particular value of the neutrino CP phase within normal mass ordering and has a visible tension with T2K's measurement while agrees at 90% confidence level in Inverted Ordering (IO). This tension may arise because of the systematic uncertainties or maybe a hint for new physics effects arising from sterile neutrinos or non-standard neutrino interactions[24–29]. Another promising long-baseline neutrino experiment under construction is DUNE (Deep Underground Neutrino Experiment)[30–35], whose goals are the determination of the neutrino mass ordering, observation of CP violation (up to 50% level), and precise measurements of oscillation parameters, such as $\delta_{\rm CP}$, $\sin^2(2\theta_{21})$. The idea is to send a wide-band high-intensity muon neutrino beam from Fermilab to the Sanford Underground Facility in Homestake at the 1300 Km distance. The detector technology of DUNE experiment is based on building liquid argon time projection chambers (LArTPC). Unlike the T2K experiment, the neutrino beam energy has a peak at 2.5 GeV with a broad range of neutrino energies. The neutrino beam is produced from proton collision on the graphite target. In the corresponding DUNE Technical Design Report (TDR)[31–33,36], it is shown that favorable values for $\delta_{\rm CP}$ with $3\sigma(5\sigma)$ can be achieved after 5 (10) years of running. It is worth noting that although muon beams produced from proton-on-target experiments like T2K, NOvA, and DUNE can have higher luminosity and energy, but there are also some disadvantages i.e., beam contamination because of the intermediate hadronic states and their decay products, higher emittance etc. It is also worth noting that produced neutrino and antineutrino beams in the above experiments can not be run at the same time, which takes much longer time than a simultaneous run of neutrino and antineutrino beams.

In this paper, we are interested in applying collimated muon beams into neutrino mixing and CP phase measurements. This motivates us to examine the physics potential of muon beams produced from lepton collider[37], especially positron-on target experiment. One example of a muon collider design is the positron-on-target method (LEMMA), which has been proposed for high-quality muon beam production[38,39]. Earlier studies using proton-on-target muon beams can be found in refs. 40–42. Although it is still quite challenging to achieve enough high luminosity for muon beam collisions[43,44], we find it quite promising for neutrino oscillation studies, with comparable or even larger neutrino flux than other long-baseline neutrino experiments. In the LEMMA approach, the incident positron energy is around 45 GeV, producing collimated muon pairs with opening angles of around 0.005 rad. and a large boost about $\gamma \sim 200$, which extends the muon lifetime by the order of $\mathcal{O}(10^2)$. Generally, the number of muon pairs produced per positron bunch on target can be expressed as

$$n(\mu^+\mu^-) = n^+\rho_{e^-} l\sigma(\mu^+\mu^-), \tag{1}$$

where n^+ is the number of e^+ in each positron bunch, ρ_{e^-} is the electron density in the medium, l is the thickness of the target, and $\sigma(\mu^+\mu^-)$ being the cross section of the muon pair production. The number of muon pairs per positron bunch on target can be maximally estimated as $n(\mu^+\mu^-)_{\rm max} \approx n^+ \times 10^{-5}$. Although the beam density is lower than the proton-on-target scenario, there are several significant benefits leading to large neutrino flux and high sensitivity on CP phase, including (1) collimated and manipulable muon beams, which lead to a larger acceptance of neutrino sources in the far detector side; (2) symmetric μ^+ and μ^- beams, and thus symmetric neutrino and antineutrino sources, which make this proposal ideally suitable for measuring neutrino CP-violating phase. We note that neutrino and antineutrino flux distributions produced from collimated muon beams are the same, and therefore, $\bar{\nu}_e \to \bar{\nu}_\mu$ and $\nu_e \to \nu_\mu$ oscillation signals can be collected simultaneously, without the need for separate runs for neutrinos or antineutrinos. We demonstrate that the estimated neutrino flux in our proposal is comparable to or larger than the DUNE experiment. The neutrino energy has wide distributions in 1–20 GeV region, and peaks at around 5–15 GeV (neutrino energy can be further tuned with on-axis and off-axis techniques), suggesting our proposal is also suitable for tau neutrino studies, because the peak energy is much greater than the threshold energy for tau lepton production. Considering both muon and electron neutrinos and antineutrinos, the signal yields indeed can be doubled or more. Finally, we point out that it is possible to exchange μ^+ and μ^- flying routes, and consequently, reducing possible bias or systematic uncertainties. We perform a prospective study mainly dealing with the CP-violation sensitivities using `GLoBES`, an open-source program for simulating standard or non-standard neutrino oscillations including matter effects[45–47]. This software is kept tested by superbeam neutrino oscillation experiments over several decades.

Results and discussion

Theory of neutrino oscillation

Here, we discuss some interesting properties of neutrino oscillation probability with regard to the energy and baseline length. We start with a general discussion regarding standard oscillation probabilities. Based on the general knowledge of quantum mechanics, we can obtain the transition amplitude as inner product of initial and final neutrino flavor states[2]. We derive appearance probability for ν_τ, ν_μ, ν_e and their antineutrinos following the general oscillation Eq. (2)

$$\begin{aligned} P(\nu_\alpha \to \nu_\beta) &= \delta_{\alpha\beta} - 4\sum_{i<j}^{n} \mathrm{Re}\left[U_{\alpha i}U^*_{\beta i}U^*_{\alpha j}U_{\beta j}\sin^2 X_{ij}\right] \\ &\quad + 2\sum_{i<j}^{n} \mathrm{Im}\left[U_{\alpha i}U^*_{\beta i}U^*_{\alpha j}U_{\beta j}\right] \sin 2X_{ij}, \end{aligned} \tag{2}$$

where $U_{\alpha i}$ are the elements of PMNS mixing matrix, and X_{ij} reads as

$$X_{ij} = \frac{(m_i^2 - m_j^2)L}{4E_\nu} = 1.267\frac{\Delta m^2_{ij}}{\mathrm{eV}^2}\frac{L}{\mathrm{Km}}\frac{\mathrm{GeV}}{E_\nu}, \tag{3}$$

L is the length of the neutrino propagation distance whose unit is Km and E_ν corresponds to the true neutrino energy in GeV unit, Δm^2_{ij} is the squared-mass difference in eV^2 unit. The oscillation probabilities for antineutrino can be obtained with the exchange $U \to U^*$. The first term in Eq. (2) is CP-conserving since it is the same for neutrinos and antineutrinos, while the last one is CP-violating because it has opposite signs for neutrinos and antineutrinos. As mentioned in "Introduction", the simultaneous run of μ^+ and μ^- beams will provide eight oscillation channels through the decay $\mu^- \to \nu_\mu + \bar{\nu}_e$ and $\mu^+ \to \bar{\nu}_\mu + \nu_e$:

$$\begin{aligned} &\nu_\mu \to \nu_\tau, \quad \bar{\nu}_\mu \to \bar{\nu}_\tau \\ &\nu_\mu \to \nu_e, \quad \bar{\nu}_\mu \to \bar{\nu}_e \\ &\nu_e \to \nu_\tau, \quad \bar{\nu}_e \to \bar{\nu}_\tau \\ &\nu_e \to \nu_\mu, \quad \bar{\nu}_e \to \bar{\nu}_\mu \end{aligned}$$

Based on Eq. (2), we can get some approximated results for the vacuum oscillation probabilities for the above eight oscillation channels as

$$\begin{aligned} P(\nu_\mu \to \nu_\tau) \simeq\ & \sin^2(2\theta_{23})\cos^4(\theta_{13})\sin^2\left(1.27\frac{\Delta m^2_{32}L}{E_\nu}\right) \\ & \pm 1.27\Delta m^2_{21}\frac{L}{E_\nu}\sin^2\left(1.27\frac{\Delta m^2_{32}L}{E_\nu}\right) \times 8J_{\rm CP}, \end{aligned} \tag{4a}$$

$$\begin{aligned} P(\nu_\mu \to \nu_e) \simeq\ & \sin^2(2\theta_{13})\sin^2(\theta_{23})\sin^2\left(1.27\Delta m^2_{32}\frac{L}{E_\nu}\right) \\ & \mp 1.27\Delta m^2_{21}\frac{L}{E_\nu}\sin^2\left(1.27\Delta m^2_{32}\frac{L}{E_\nu}\right) \times 8J_{\rm CP}, \end{aligned} \tag{4b}$$

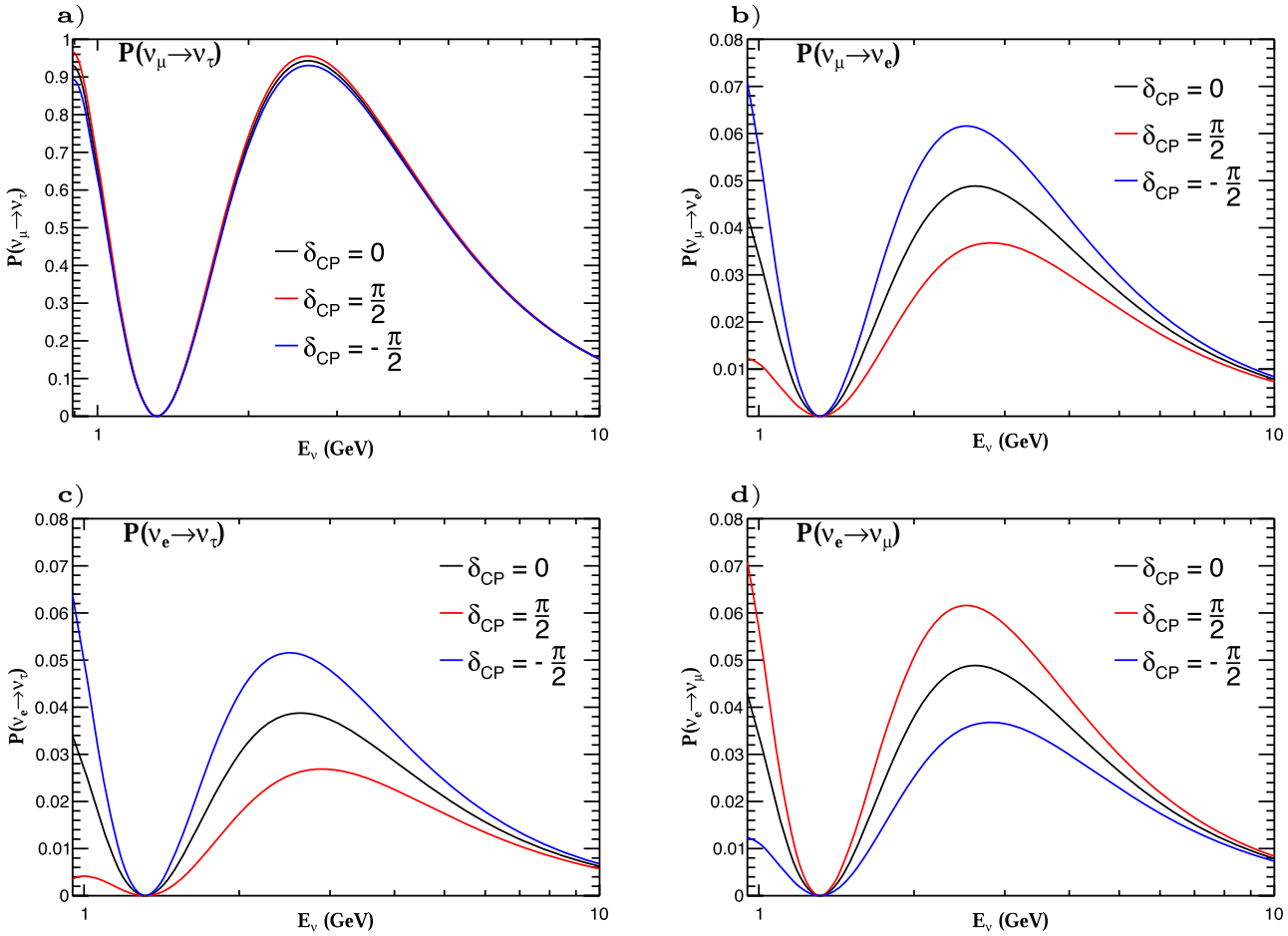

Fig. 1 | The vacuum oscillation probabilities (vertical axis) of neutrinos as a function of neutrino energy E_ν. **a** Muon neutrino (ν_μ) oscillation into tau neutrino (ν_τ). **b** ν_μ oscillation into electron neutrino (ν_e). **c** $\nu_e$oscillation into ν_τ. **d** ν_e oscillation into ν_τ. The baseline length of the neutrino oscillation is set to L = 1300 Km. The oscillation probability is corresponding to three different charge-parity violation phase values δ_{CP}: black line for $\delta_{CP} = 0$, red line for $\delta_{CP} = \pi/2$, and blue line is for $\delta_{CP} = -\pi/2$.

$$P(\nu_e \to \nu_\tau) \simeq \sin^2(2\theta_{13})\cos^2(\theta_{23})\sin^2\left(1.27\Delta m^2_{32}\frac{L}{E_\nu}\right) \mp 1.27\Delta m^2_{21}\frac{L}{E_\nu}\sin^2\left(1.27\Delta m^2_{32}\frac{L}{E_\nu}\right)\times 8J_{CP}, \quad (4c)$$

$$P(\nu_e \to \nu_\mu) \simeq \sin^2(2\theta_{13})\sin^2(\theta_{23})\sin^2\left(1.27\Delta m^2_{32}\frac{L}{E_\nu}\right) \pm 1.27\Delta m^2_{21}\frac{L}{E_\nu}\sin^2\left(1.27\Delta m^2_{32}\frac{L}{E_\nu}\right)\times 8J_{CP}, \quad (4d)$$

where J_{CP} is the Jarlskog invariant[48] and replacing the mixing parameters with up-to-date measured values[49],

$$J_{CP} \equiv \sin\theta_{13}\cos^2\theta_{13}\sin\theta_{12}\cos\theta_{12}\sin\theta_{23}\cos\theta_{23}\sin\delta_{CP} = 0.03359 \pm 0.0006(\pm 0.0019)\sin\delta_{CP}. \quad (5)$$

It should be pointed out that we drop the sub-leading terms, second order in $\sin\theta_{13}$ and Δm^2_{21} in the above oscillation probabilities. The above form of the oscillation probabilities are applicable for most of the superbeam experiments without the consideration of the matter effects. However, this form of oscillations might differ from the results obtained with GLoBES. The vacuum oscillation probabilities in Eq. (4a–d) are plotted in Fig. 1 with respect to the neutrino energy in the 1 GeV < E_ν < 10 GeV range. Figure 1a, b represents the $P(\nu_\mu \to \nu_\tau)$ and $P(\nu_\mu \to \nu_e)$, while Fig. 1c, d shows the oscillation probabilities of ν_e into ν_μ and ν_τ. The probability for antineutrino oscillations can be obtained by simply replacing δ_{CP} with $-\delta_{CP}$. The oscillation probability difference between $P(\nu_\alpha \to \nu_\beta)$ and $P(\bar{\nu}_\alpha \to \bar{\nu}_\beta)$ reads as

$$\Delta P(\nu_\alpha \to \nu_\beta) = 16J_{CP} \times 1.27\Delta m^2_{21}\frac{L}{E_\nu}\sin^2\left(\frac{\Delta m^2_{32}L}{E_\nu}\right). \quad (6)$$

Using the current measured values of the mixing angles and squared-mass differences[49] and taking the distance of neutrino propagation as $L = 1300$ Km, we have the numeric values for the neutrino oscillations at $E_\nu = 7$ (5) GeV as

$$P(\nu_\mu \to \nu_\tau) = 0.2916 \pm 0.0026\sin\delta_{CP}\,(0.5093 \pm 0.0048\sin\delta_{CP}), \quad (7a)$$

$$P(\nu_\mu \to \nu_e) = 0.0151 \mp 0.0026\sin\delta_{CP}\,(0.0264 \mp 0.0048\sin\delta_{CP}), \quad (7b)$$

$$P(\nu_e \to \nu_\mu) = 0.0151 \pm 0.0026\sin\delta_{CP}\,(0.0264 \pm 0.0048\sin\delta_{CP}), \quad (7c)$$

$$P(\nu_e \to \nu_\tau) = 0.0119 \mp 0.0026\sin\delta_{CP}\,(0.0209 \mp 0.0048\sin\delta_{CP}). \quad (7d)$$

The impact of matter effects on the appearance probability may be negligible in the short-baseline oscillation experiments and for reactor neutrinos, in which the general formula (2) can be applicable. Given the significant length of the oscillation baseline in our proposal, matter effects arising from the interaction of neutrinos with nucleons of matter as they propagate through

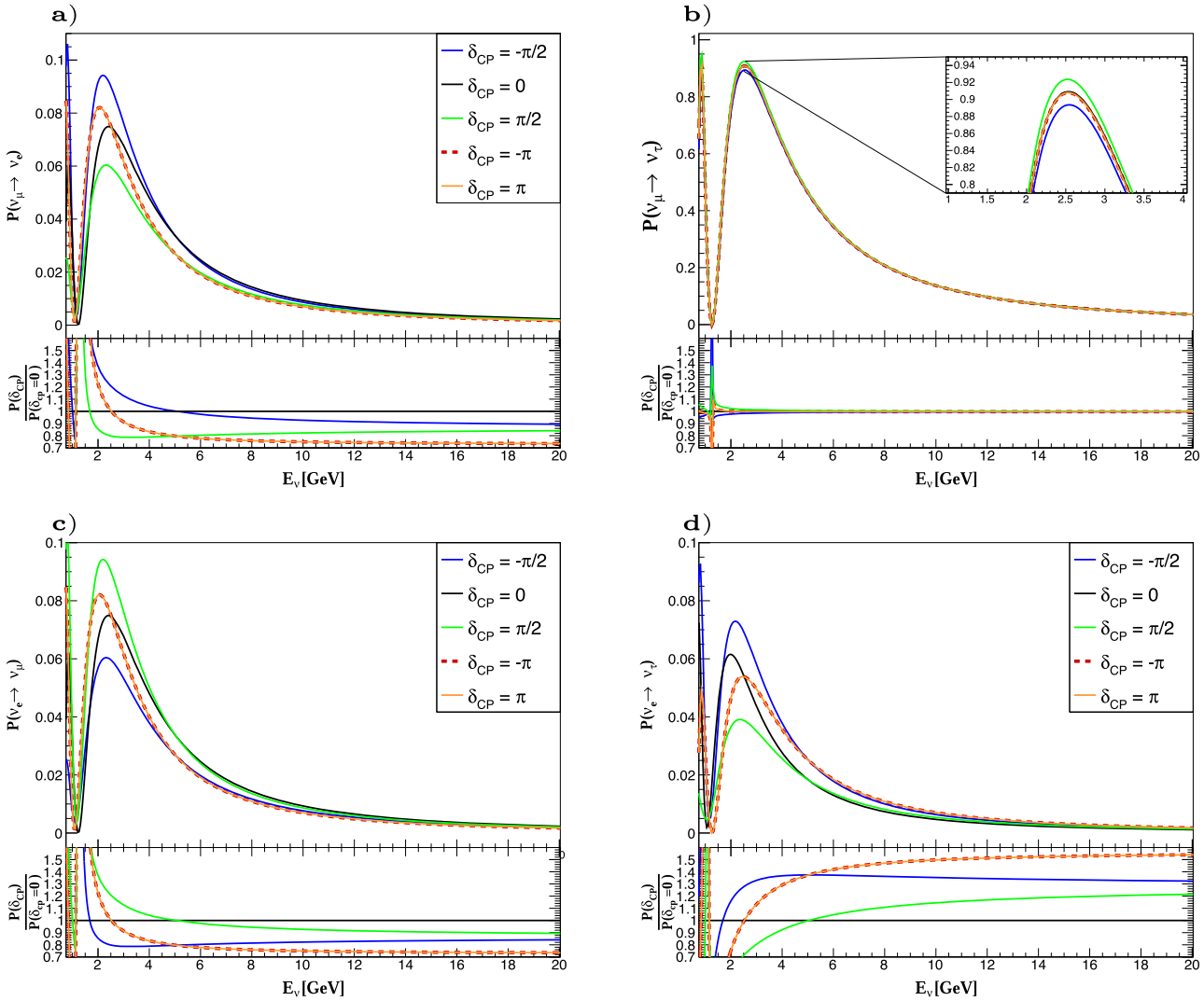

Fig. 2 | Matter oscillation probabilities of neutrinos as functions of neutrino energies E_ν. **a**, **b** display oscillation probability (vertical axis) for muon neutrino (ν_μ) into electron neutrino (ν_e) and tau neutrino (ν_τ). The little icon in (**b**) depicts the peak of the $\nu_\mu \to \nu_\tau$ oscillation probability. **c**, **d** depict oscillation probabilities for ν_e into ν_μ and ν_τ. Probabilities are drawn with respect to the neutrino reconstructed energy and depicted for five δ_{CP} values: $\delta_{CP} = -\pi/2, 0, \pi/2, -\pi, \pi$ given in blue, black, green, dashed red and orange lines. In each plot, the ratio $P(\delta_{CP} \neq 0)/P(\delta_{CP} = 0)$ is shown in the small bottom panel. The length of oscillation baseline is taken as $L = 1300$ Km, and normal mass ordering is assumed.

the Earth's internal crust should be taken seriously, because the matter-induced correction factor for the oscillation probability is relatively larger than other short-baseline oscillation experiments[50,51]. This may bring some visible changes to our vacuum oscillation probabilities shown in the Fig. 1. A complete set of neutrino oscillation probabilities, including matter effect with constant density for three flavors, are analytically calculated through series expansions in the mass hierarchy parameter, $\Delta m^2_{21}/\Delta m^2_{31}$, and mixing parameter sin θ_{13} with first and second order, which is available in ref. 52.

Now we demonstrate the appearance probabilities for $P(\nu_\mu \to \nu_e)$, $P(\nu_\mu \to \nu_\tau)$, $P(\nu_e \to \nu_\mu)$, $P(\nu_e \to \nu_\tau)$ channels that depict the impact of matter effects on the neutrino oscillation. The probability is the function of the reconstructed neutrino energy and drawn for five fixed δ_{CP} values as shown in the Fig. 2. The overall size of the probabilities are almost the same for $P(\nu_\mu \to \nu_e)$, $P(\nu_e \to \nu_\mu)$, $P(\nu_e \to \nu_\tau)$, shown as in Fig. 2a, c, d. However, the oscillation probability $P(\nu_\mu \to \nu_\tau)$ depicted in Fig. 2b is much greater than the other three probabilities thus enhances the ν_τ neutrino-related events at the far detector. From the ratio of probabilities with nonzero δ_{CP} to probabilities with $\delta_{CP} = 0$, $P(\delta_{CP} \neq 0)/P(\delta_{CP} = 0)$, it is very clear that the inclusion of matter effects change the shapes of oscillation probability significantly relative to the vacuum oscillations. Two of the five δ_{CP} values, $-\pi/2$ (blue line) and $\pi/2$ (green line), maximize the CP violation the most while the other three values are thought to be CP-conserving phase: π (orange line), $-\pi$ (red dashed line), 0 (black line). Therefore, oscillation probability is supposed to be the same for these three CP-conserving δ_{CP} values. However, there is a difference between them: $P(\delta_{CP} = 0) \neq P(\delta_{CP} = -\pi) = P(\delta_{CP} = \pi)$. This may arise from the collective influence of the matter effects and the expansion method. It is worth noting that, for the oscillation channels $P(\nu_\mu \to \nu_e)$ and $P(\nu_e \to \nu_\mu)$, the probability with $\delta_{CP} = 0$ is larger than that of the other δ_{CP} values. As for the tau neutrino appearance from ν_μ and ν_e channels, the outcome is different. In the $\nu_\mu \to \nu_\tau$ oscillation channel, the difference of the oscillation probability for CP-conserving δ_{CP} values is very small or even becomes zero as the neutrino energy increases. We will see further outcome with both the event spectrum and significance in the following sections.

Experimental setup and qualitative estimations

We display in Fig. 3 a rough structure of neutrino oscillation experiment to probe neutrino CP phase by measuring muon electron (anti-)neutrino mixing and their differences. We are especially interested in the oscillation modes of $\nu_\mu \to \nu_{e,\tau}$, $\nu_e \to \nu_{\mu,\tau}$ and their corresponding antineutrinos with

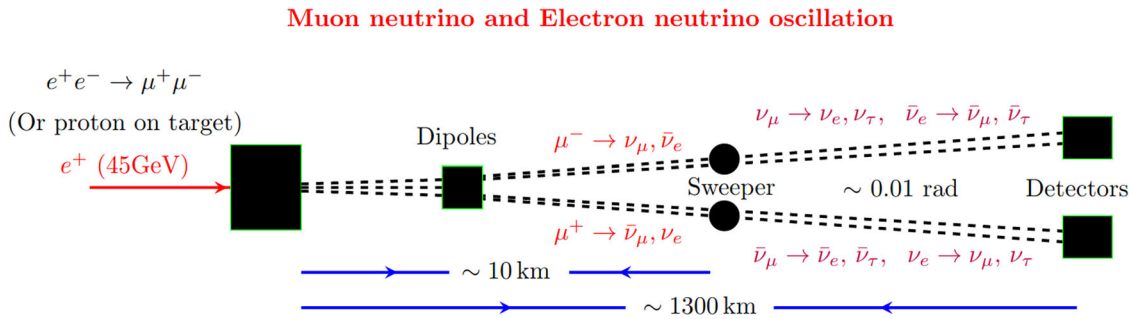

Fig. 3 | A proposed neutrino oscillation experiment to probe charge-parity violating phase through muon electron (anti-) neutrino oscillation and the differences of resulted $\nu_{e,\mu} \to \nu_\tau$, $\nu_e \to \nu_\mu$, and their antineutrino correspondents. This proposal is based on collimated muon beams achieved from e.g., Positron-on-Target method, where 45 GeV positron beams are fired. Dipoles are used to separate muon (μ^+) and antimuon (μ^-) with an angle around 0.01 rad., with direction changeable. Muon beams fly about 10 Km and radiate neutrinos before being swept away by the Sweeper. Neutrinos then further fly 1300 Km to reach DUNE type of detectors.

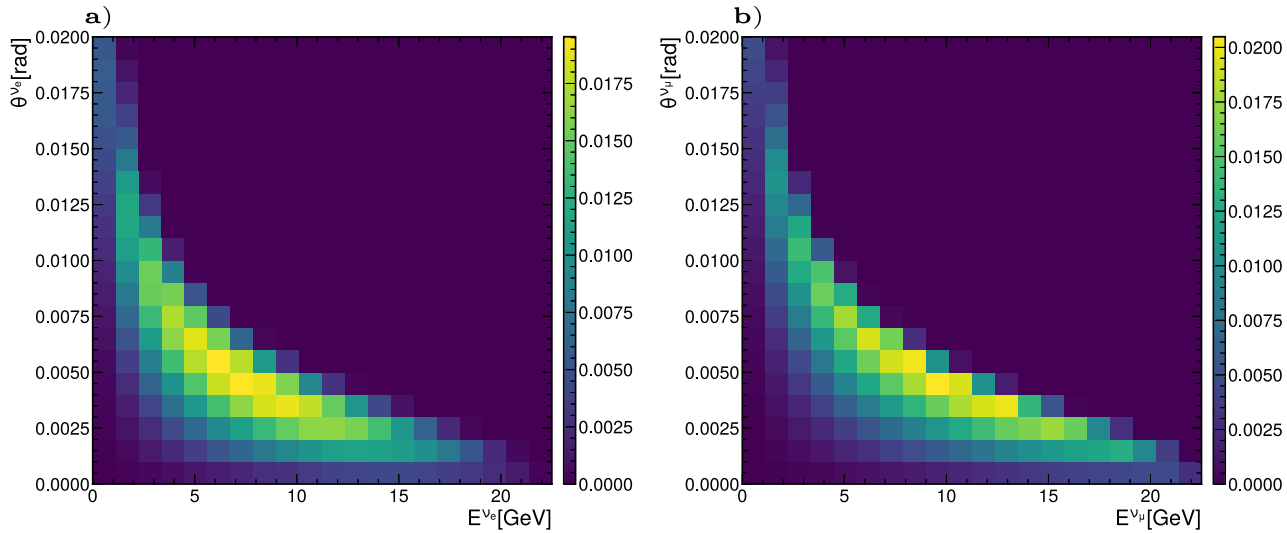

Fig. 4 | 2D distributions of energy and angle. a is for electron neutrino ν_e and **b** is for muon neutrino ν_μ. Neutrinos are coming from 22.5 GeV $\mu^+ \to e^+ \bar{\nu}_\mu \nu_e$ (similarly for μ^- decay) in respect to muon flying direction. The color bar in each panel represents normalized density distributions for each type of neutrinos.

more details to be given later. This proposal is based on collimated muon beams achieved from e.g., Positron-on-Target method, where 45 GeV positron beams are shed on the target. Dipoles are used to separate μ^+ and μ^- with an angle around 0.01 rad., with direction changeable (notice the acceptance of the dipole to separate muon and anti-muons is not considered here and needs to be evaluated later). Muon beams fly about 10 Km and radiate neutrinos before being swept away. Neutrinos then further fly e.g., 1300 Km to reach DUNE or T2K type of detectors[31].

- Muon production rates. As estimated in the Eq. (1), the produced muon numbers is $n(\mu^+\mu^-)_{max} \approx n^+ \times 10^{-5}$[39]. Assuming positron bunch density as 10^{12}/bunch and bunch crossing frequency as 10^5/s, we get muon production rates $dN_\mu/dt \sim 10^{12}$/s (or 10^{19}/year). Notice although we take positron-on-target muon source as an example, proton-on-target muon beams should also be applicable. Moreover, the future TeV scale muon collider is indeed targeting a much larger intensity beam by more than 1–2 orders of magnitudes[43,44,53].
- For muons with the energy around 20 GeV, the mean flying distance is around 100 Km. If there is a straight tube with a length around 5–10 Km to let muons go through with quadrupoles to keep them merged (To further reduce the angular emittance with quadrupoles is to be checked), the decayed fraction can reach 10^{-1} in realistic case. On the other hand, we can also refer to a muon complex as discussed in ref. 54, where the muon beam is accelerated in a circular section and then extracted into the rectangular section for decays. The intensity of the neutrino beam compared with the incoming muon beam is suppressed by a ratio around 10^{-1}, i.e., the fraction of the collider ring circumference occupied by the production straight section.
- The opening angles between muon beams axis and the momentum of decay products are around 0.005 rad. as shown in Fig. 4a and may be kept smaller with quadrupoles. For neutrinos traveling 1300 Km to reach far detector s, the spread size can be around 1–5 Km. For a DUNE-like detector with a cubic size of about 20 m[31], the neutrino acceptance is then 10^{-4}.
- Neutrino and antineutrino interactions inside detectors. With a $L = 20$ m long liquid Argon detector (DUNE far detector indeed has a length around 50 m[31]), the expected event yield rate can be roughly estimated with: $dN_\mu/dt \times L \times \sigma_{n\nu} \times \rho N_A \cdot dE$, where N_A is the Avogadro constant, $\rho \sim 2.834$ gcm^{-3}, $\sigma_{n\nu}$ represents the neutrino-nucleon cross sections and is ~10^{-38} cm^2 for a 10 GeV neutrino[49,55]. Actually, the cross sections are function of the neutrino energy energy. We will show the simulated results for neutrino cross sections in below sections.

Because of its heavy mass and very short lifetime, the tau neutrino production with abundant numbers in conventional accelerator is very difficult. On the contrary, we have rich tau neutrino flux because of the higher $P(\nu_\mu \to \nu_\tau)$ oscillation shown in Fig. 1b. The tau neutrino flux can be further strengthened if we consider the oscillation channel of $P(\nu_e \to \nu_\tau)$ whose oscillation probability is much more smaller than $P(\nu_\mu \to \nu_\tau)$. Considering the fraction of muon neutrino oscillated into tau neutrino[56], we can

estimate the total tau neutrino CC events based on the Eq. (7) with 5 years of run as

$$N^{cc}_{\nu_\tau} \sim (3 \times 10^4). \tag{8}$$

Notice the annual expected tau neutrino yields is already comparable or even surpass the rates at the SHiP experiment at CERN[57]. Thus our proposal can serve as a "brighter" neutrino factory for tau neutrinos. We would like to mention that with this abundance in neutrinos fluxes, it may possible that some of the new physics models, such as charged Higgs doublet[58] or leptoquarks[59] maybe tested through new generation lepton collider[60] whose colliding beams are produced with the electron–positron collision.

Given the differences in cross sections for neutrinos and antineutrinos, we simulate the interactions of neutrinos with Argon atoms with a mass number of 40 using the GENIE[61–63] event generator version 3.2.0 to obtain neutrino and antineutrino cross sections. Indeed, the cross sections for neutrinos and antineutrinos differ as the neutrino energy increases. Figure 5 shows the total Charged-Current (CC) cross sections of three neutrino and antineutrino flavors with respect to neutrino energy. The total cross sections

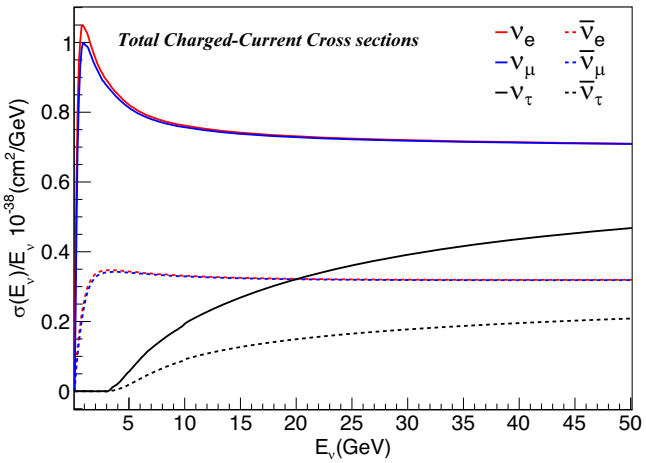

Fig. 5 | Neutrino and antineutrino Charged-Current (CC) cross sections with Argon Atom of mass number 40. The solid lines represent the cross sections of neutrino and nucleon interaction while the dashed lines are for antineutrino-nucleon cross sections. Red solid and dashed lines depict ν_e and $\bar{\nu}_e$ cross sections. Blue solid and dashed lines represent ν_μ and $\bar{\nu}_\mu$ cross sections while black solid and dashed lines present ν_τ and $\bar{\nu}_\tau$ cross sections.

should be understood as the sum of cross sections for available CC interactions of the neutrinos with nucleons of the Argon atom. The solid lines refer to neutrino-nucleon cross sections while the dashed lines represent cross sections of antineutrino-nucleon interactions. The simulated results for cross sections are consistent with those of DUNE's experimental configuration[34], except for the ν_τ cross sections, because the DUNE experiment mainly focuses on the $\nu_\mu \rightarrow \nu_e$ oscillation channel. It is worth noting that the cross sections in Fig. 5 are normalized with respect to energy. Naturally, the neutrino-nucleon CC cross section is linearly dependent on the energy until the energy reaches the threshold of the W boson. One particularly important feature is that antineutrino cross sections are approximately half the size or even smaller than the neutrino cross sections, which has a significant impact on the final event spectrum.

As the oscillation route for neutrinos is significantly longer than other short-baseline experiments, such as MOMENT[64], the matter effects during oscillations should be taken into account. To maintain consistency with the neutrino oscillation probabilities, we utilize the matter-affected oscillation probability formulas coded within GLoBES.

Results of simulation and CP sensitivity

Figure 6 depicts event distribution as function of δ_{CP} for ν_e appearance from ν_μ in Fig. 6a and the ratio of our results to that of the DUNE in Fig. 6b (solid red line) at different parent muon energies, ranging from 2.5 to 15 GeV. The red solid line corresponding to DUNE TDR is obtained by simulation using the DUNE's experimental configuration given in ref. 34. We show this because at the lower energy the oscillation patterns and thus the event spectrum for neutrinos in our case is identical to those of the DUNE experiment while they are visibly different toward higher energy. The event rates for electron neutrino obtained with our proposal is approximately seven to eight times larger than DUNE's ν_e event rates as shown on ratio plot.

The event distributions as a function of reconstructed neutrino energy are shown in Fig. 7 for $\delta_{CP} = 0$ (black line), $\pi/2$ (red line), $-\pi/2$ (blue line). The maximum numbers of events for all channels have peaks approximately at 15 GeV. Figure 7a–d displays tau and anti-tau neutrino appearance from muon and antimuon oscillation channels. Figure 7e, f displays electron and anti-electron appearance rate from muon and antimuon oscillation channels. The last two panels of Fig. 7g, h depict muon and antimuon appearance rate from electron and anti-electron oscillation channels. From the shapes of event distributions for $\nu_\mu \rightarrow \nu_\tau$ channel shown in Fig. 7a, we can find that events of three different δ_{CP} values are not visibly different for ν_τ appearance form ν_μ oscillation, which makes the sensitivity from this channel weaker than other appearance channel. However, events from the other channels are apparently differentiable for $\delta_{CP} = 0, \pi/2, -\pi/2$, which is

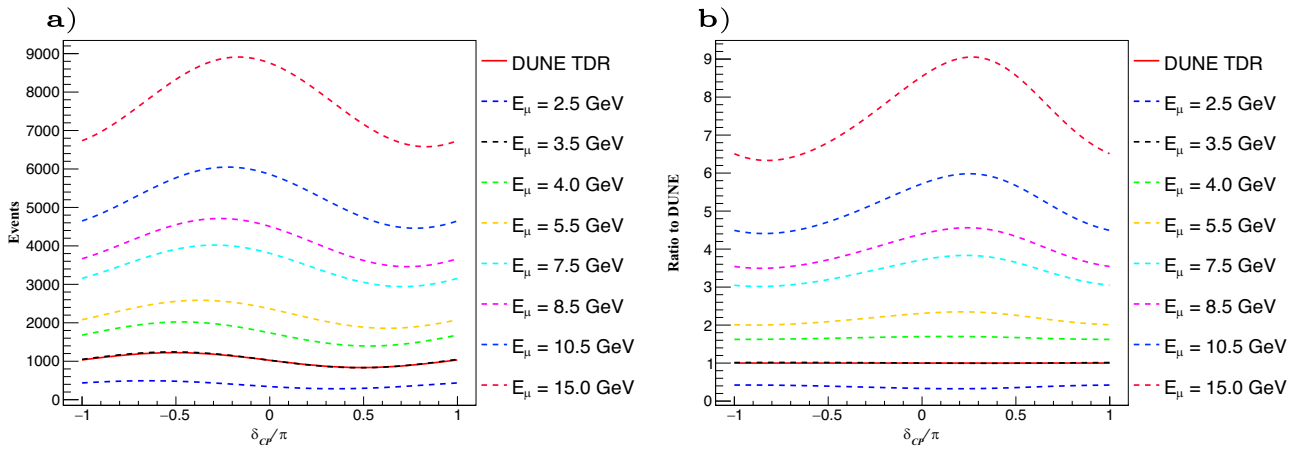

Fig. 6 | Event distribution as a function of charge-parity violation factor. a Event distributions at different parent muon energies E_μ. **b** Ratio of event distributions of our experimental setup to that of the DUNE experiment. Events are only taken for electron neutrino (ν_e) appearance from muon neutrino (ν_μ) oscillation. The red solid line in both plots stand for the simulated results using DUNE's experimental configurations while other dashed lines depict our results at different muon energies.

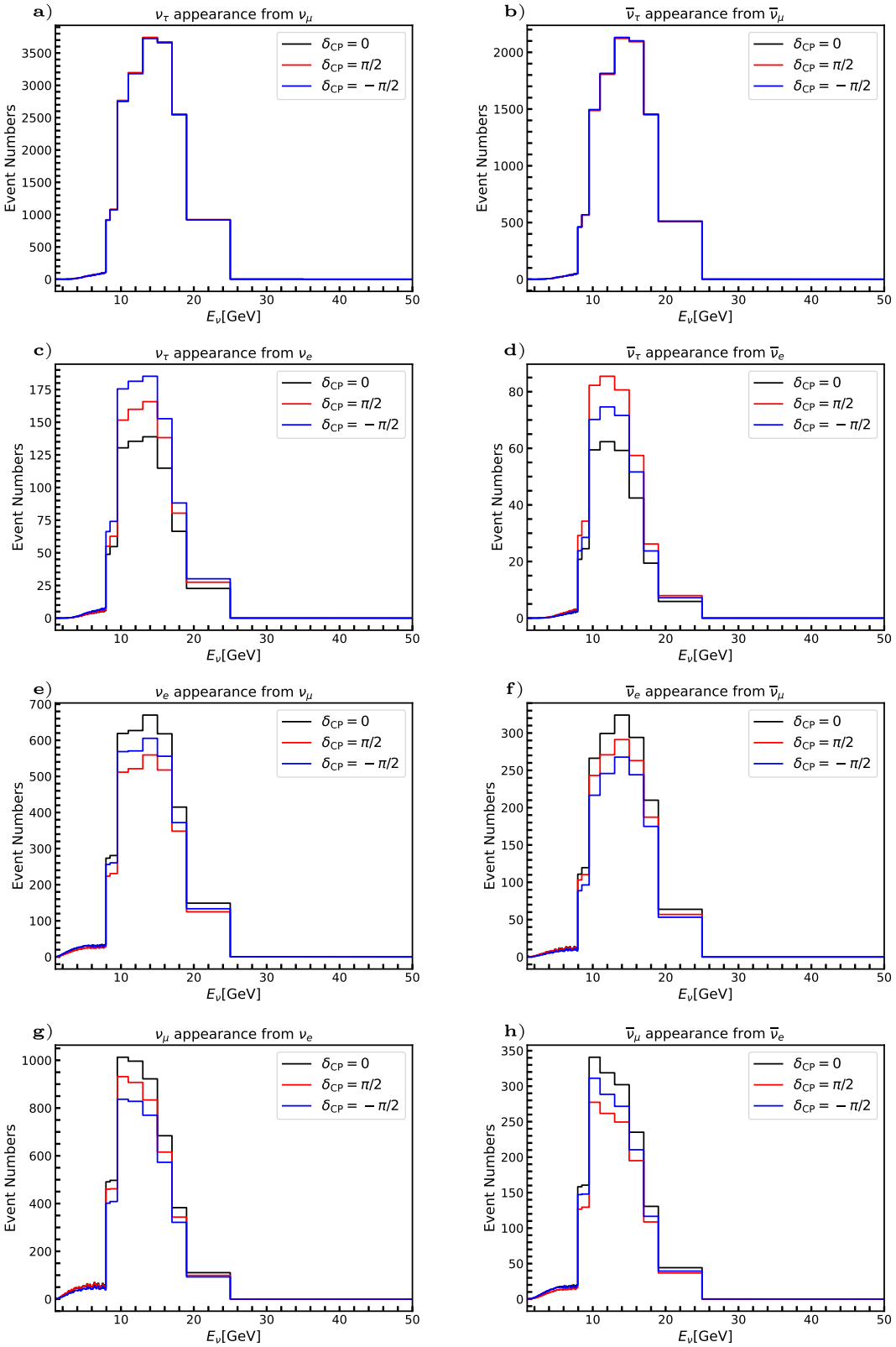

Fig. 7 | Event spectrum as function of reconstructed neutrino energy E_ν. **a**–**d** show (anti)tau neutrino ($\nu_\tau/\bar{\nu}_\tau$) appearance rate from muon and electron (anti)neutrino ($\nu_\mu/\bar{\nu}_\mu, \nu_e/\bar{\nu}_e$). **e**, **f** display $\nu_e/\bar{\nu}_e$ appearance rate from $\nu_\mu/\bar{\nu}_\mu$ oscillation channel, while **g**, **h** display $\nu_\mu/\bar{\nu}_\mu$ appearance rate from electron and anti-electron neutrino. Events are obtained with a 5-year of run simultaneously for neutrino and anti-neutrino mode with normal mass ordering is assumed for three charge-parity violating phase (δ_{CP}) values: $\delta_{CP} = 0$ (black line), $\delta_{CP} = \pi/2$ (red line), $\delta_{CP} = -\pi/2$ (blue line).

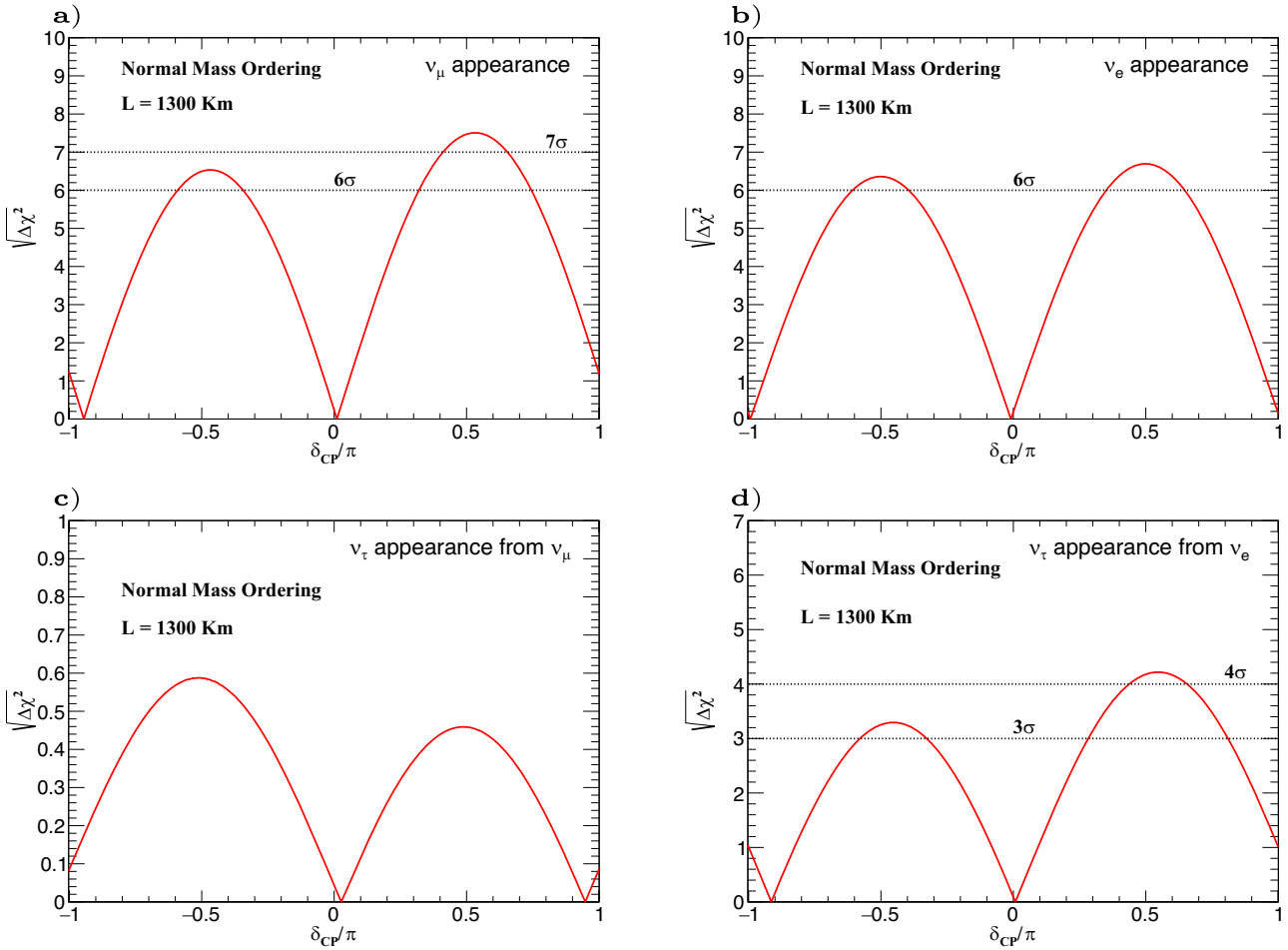

Fig. 8 | The significance χ^2 for the determination of charge-parity (CP) violation as a function of the value of the δ_{CP}. **a** Muon neutrino (ν_μ) appearance channel. **b** Electron neutrino (ν_e) appearance channel. **c**, **d** Tau neutrino (ν_τ) appearance channel form ν_μ and ν_e oscillations. L is the neutrino propagation distance during oscillation. The normal mass ordering is assumed during the analysis.

good for obtaining a high sensitivity for δ_{CP}. As shown clearly, the event spectra for neutrino appearance are almost double of the number of anti-neutrino events since the cross section of neutrino interaction is significantly larger than the antineutrino cross sections. It is worth noting that events produced for $\delta_{CP} = 0$ is less than $\delta_{CP} = \pi/2, -\pi/2$ for $\nu_e \to \nu_\tau$. On the other hand, case is opposite for $\nu_\mu \to \nu_e$ and $\nu_e \to \nu_\mu$ channels. This is different from the low-energy neutrino oscillation experiments e.g., T2K, NOvA etc, whose event distributions are in increasing (for neutrino) or decreasing (for antineutrino) order for δ_{CP} values. This is because of the different oscillation patterns at the high energy shown in the Fig. 1.

We will now show the results of the sensitivities on neutrino CP violation on Fig. 8, taking $\delta_{CP} = \pm\,\pi/2$ as benchmark parameters:

- First, if the far detector has the capability of distinguishing electron and muon neutrino from one another, then both the ν_μ and ν_e appearance channel can provide a high CP sensitivity. The sensitivity results are displayed in Fig. 8. The left-panel of the figure depicts estimated sensitivity for ν_μ appearance channel while the figure on the right-hand side display estimated sensitivity for ν_e appearance channel. It is clear that ν_μ appearance channel has the potential to discover CP violation up to 7σ sensitivity at $\delta_{CP} = \pi/2$ while there is also sensitivity for $\delta_{CP} = -\pi$ and π with more than 1σ. On the other hand, the ν_e appearance channel can also provide discovery of the maximum CP violation with more than 6σ significance.
- Second, one of the advantages of our proposal is that we can also gain sensitivity in the case of detecting ν_τ-related events. It is well-known fact that observing tau neutrino is extremely difficult. Luckily, DUNE-type detectors can handle this problem. Figure 8c depicts the significance of ν_τ appearance from ν_μ oscillation. As seen, for five years of run, this sensitivity is very small because the event rate for $\delta_{CP} = 0, -\pi, \pi$ are not visibly different, depicted as in Fig. 7a, b. However, Fig. 8d displays δ_{CP} sensitivity for the ν_τ appearance from ν_e oscillation channel. The corresponding significance can rich up to 4σ, although this channel is not as good as the first two appearance channels for obtaining better sensitivity. Notice that the CP dependence of $P(\nu_e \to \nu_\tau)$ and $P(\bar{\nu}_\mu \to \bar{\nu}_\tau)$, as shown in Eq. (4), vary in the same direction. If we count on tau-related events in the far detector inclusively, this means ν_τ signal can be further strengthened. The sensitivity then can be more than 4 standard deviations. Although only statistics are taken into account here, systematic uncertainty could be reduced efficiently due to the symmetric property of the proposed device. Furthermore, it is possible to exchange μ^+ and μ^- flying routes, thus further reducing possible bias or systematic.
- Finally, if we analyze total ν_τ event spectrum from muon and electron neutrino oscillations as:

$$\mu^+ \to e^+\,\bar{\nu}_{\mu 1}\,\nu_{e1} \;\Rightarrow\; \bar{\nu}_{\mu 1} \to \bar{\nu}_{\tau 1},\ \nu_{e1} \to \nu_{\tau 1},$$
$$\mu^- \to e^-\,\nu_{\mu 2}\,\bar{\nu}_{e2} \;\Rightarrow\; \nu_{\mu 2} \to \nu_{\tau 2},\ \bar{\nu}_{e2} \to \bar{\nu}_{\tau 2},$$

we can obtain sensitivity for maximum CP violation more than 4σ if the detector efficiency ideally 100%. Figure 9 displays obtained sensitivity for CP-violating phase with two different detector efficiencies: a 100% (red line) and DUNE's simulated efficiency (black line).

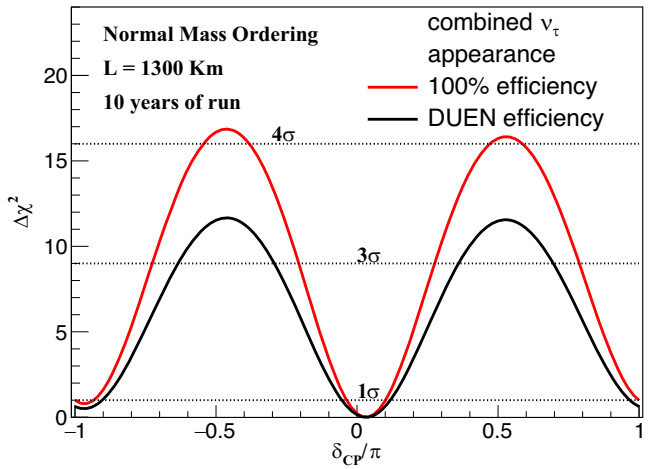

Fig. 9 | Charge-parity violating phase (δ_{CP}) sensitivity obtained with the fit from total tau neutrino ν_τ appearance channel. Corresponding events are obtained with 10 years of run and assuming normal mass ordering. The red line represents obtained sensitivity with nearly 100% efficiency in each energy bin while the black line represents sensitivity obtained using DUNE-provided energy efficiency that comes with their experimental configuration file.

Feasibility for sterile neutrino search

The existence of the fourth neutrino, or sterile neutrino, is another major problem whose discovery may solve a plethora of Beyond Standard Model (BSM) mysteries, such as the origin of neutrino mass, discovering Dark Matter (DM) particles, and even the cosmological structure of the universe. It is commonly known that the Z gauge boson can decay into a pair of neutrinos and antineutrinos. Thus, the measurements of the Z boson decay width help determine the active neutrino count to be 3[65]. However, there is a possibility that sterile neutrinos are also allowed, given that they are singlets of the SM gauge group and do not directly interact with SM gauge bosons. Generally, only one sterile neutrino ν_s is considered, consisting mainly of the heavy mass eigenstate ν_4, while the SM active neutrinos are mainly composed of the light neutrino mass eigenstates, ν_1, ν_2, ν_3. Sterile neutrinos naturally appear in many extensions of the SM. Meanwhile, several experimental hints of their existence exist. As is well-known, the GALEX and SAGE solar neutrino Gallium experiments reported that only 88 ± 5% of the expected number of ν_e events were observed[66,67]. The deficit of ν_e events observed in these experiments can be explained by electron neutrino to sterile neutrino oscillation at short-baseline. The explanation of the LSND and MiniBooNE experimental results could also indicate the possible existence of sterile neutrinos[68–70].

There is one more advantage of our proposal when it comes to searching for sterile neutrinos. The rich flux of both muon and electron-type neutrinos produced after muon decay increases the possibility of observing oscillations related to sterile neutrinos. We can examine two oscillation modes simultaneously: $\nu_e \to \nu_e$ and $\nu_\mu \to \nu_e$, while DUEN and T2K mainly focus on electron neutrino appearance, $\nu_\mu \to \nu_e$. The probability of disappearance and appearance for a neutrino flavor α, taking into only the large mass difference account, can be approximated as

$$P(\nu_\alpha \to \nu_\alpha) \approx 1 - 4|U_{\alpha 4}|^2(1 - |U_{\alpha 4}|^2)\sin^2\left(\frac{\Delta m^2_{41} L}{4E_\nu}\right) \quad (9)$$

$$P(\nu_\alpha \to \nu_\beta) \approx 4|U_{\alpha 4}|^2|U_{\beta 4}|^2\sin^2\left(\frac{\Delta m^2_{41} L}{4E_\nu}\right) \quad (10)$$

With the fourth neutrino, the PMNS matrix is a 4×4 matrix that contains six mixing angles and three CP phases. Determination of these parameters would be a huge work that requires large number of neutrino oscillation experiments. According to some research work dealing with long-baseline neutrino oscillations in the presence of the sterile neutrino[71], our proposal not only enables us to further confirm the results of the LSND and MiniBooNE experiment but also help us to determine the aforementioned parameters, especially Δm^2_{41}, active and sterile neutrino mixing angles, as well as the additional CP phases. A detailed study for examining sensitivities of the parameters characterizing sterile neutrino will be presented in our future work.

Conclusion

In this work, we present a scenario that exploits collimated muon beams. We take positron-on-target as an example method to produce these beams, but this can also be based on high-energy muon beams from the proton-on-target method, which generate symmetric neutrino and antineutrino sources: $\mu^+ \to e^+ \bar{\nu}_\mu \nu_e$ and $\mu^- \to e^- \nu_\mu \bar{\nu}_e$. Interfacing with long-baseline neutrino detectors such as DUNE or Hyper-K detectors, this experiment can be useful for measuring tau neutrino properties and, importantly, for probing the neutrino CP phase by measuring ν_e, ν_μ, and ν_τ appearance, and differences between neutrino and antineutrino rates. Through simulation using GLoBES software, the CP violation sensitivities with the appearance of all three flavor neutrinos have been explored. Technically, there are several significant benefits leading to a large neutrino flux and high sensitivity to the CP phase. First, the collimated and manipulable muon beams may lead to a larger acceptance of neutrino sources on the far detector side. Second, symmetric production of μ^+ and μ^- beams also leads to symmetric neutrino and antineutrino production, which makes this proposal ideally suited for measuring neutrino CP violation. More importantly, $\bar{\nu}_{e,\mu} \to \bar{\nu}_\tau$ and $\nu_{e,\mu} \to \nu_\tau$, as well as $\bar{\nu}_e \to \bar{\nu}_\mu$ and $\nu_e \to \nu_\mu$ oscillation signals, can be collected simultaneously without the need for separate specific runs for neutrinos or antineutrinos. Therefore, our experiment can save a significant amount of time. It is also possible to exchange μ^+ and μ^- flying routes, thus further reducing possible bias or systematic errors. The discovery of CP violation in our approach is quite significant when focusing on the first two flavor neutrino appearances, with a significance of more than 6σ, or for the total appearance, which can be as high as 7σ within five years of operation. However, this requires distinguishing between electron and muon neutrinos, which although difficult, is achievable.

Moreover, the tension between T2K[18,21] and NOvA[22] results on neutrino CP measurement may reappear, making an independent probe indispensable. For example, through tau neutrino appearance or electron-to-muon neutrino oscillations. The proposal here should also be useful for detecting new CP phases in case of the presence of a sterile neutrino[72]. Last but not least, our proposal exploits a muon beam with looser requirements (e.g., lower intensity) compared to the needs for a future muon collider and thus can serve as a realistic intermediate step.

In this draft, we primarily provide preliminary estimations, either qualitative or based on existing data, for the feasibility study. A more detailed study is surely necessary to follow up this preliminary work. However, there also exists rich potential to be further explored with such a proposal that connects the energy and neutrino frontiers. Especially, one can imagine a post-DUNE (or running in parallel to DUNE as the probe channels are indeed orthogonal and thus complementary) experiment with neutrinos from an intense muon source located at the Fermilab site. This connection between energy and neutrino frontiers can also serve as a precursor for future high-energy muon colliders. Notice that a muon collider requires 1–2 orders of magnitude more intense beam compared to the number ($dN_\mu/dt \sim 10^{12}$/s) listed above as our benchmark. Thus, with the development of a more intensive muon beam targeting future muon colliders, it surely will further improve the neutrino potential of the current proposal.

Methods

In this section, we show the techniques used to analyze the event spectrum produced with the help of GLoBES. We use muon and antimuon beams produced from highly energetic positron collision with a high electron density target. Neutrinos then are produced from muon decay. We have four neutrino flavors that provide eight appearance channel. We are only

Table 1 | The parameters used for neutrino oscillations

Parameter	True value	Marginalization range
$\sin^2\theta_{12}$	0.310	Not marginalized
$\sin^2\theta_{13}$	0.0241	[0.01, 0.03]
$\sin^2\theta_{23}$	0.58	[0.38, 0.64]
δ_{CP}	$(0, \pi)$	$[-\pi, \pi]$
Δm^2_{21} (eV^2)	7.39×10^{-5}	Not marginalized
Δm^2_{31} (eV^2)	2.449×10^{-3}	Not marginalized

The first column lists the three neutrino mixing angles: θ_{12}, θ_{13}, θ_{23}, and charge-parity violating phase δ_{CP},and the two squared-mass difference Δm^2_{21}, Δm^2_{31}. The second column represents true values of these parameters for data simulation in GLoBES, while third column explains whether these parameters are free or fixed for minimizing the χ^2 function. Parameter that are not marginalized is understood as fixed or free in other case.

Table 2 | The experimental setup used in GLoBES for simulation

Experimental parameters	Values
Stored muons	1×10^{20}
E_μ[GeV]	22.5 GeV
Run time	5 years
Matter density	2.8 gcm^{-3}
Baseline length	1300 Km
Target mass (detector)	40 Kt liquid Argon

The first column shows parameters related to the experimental configuration during simulation: the number of active muons (Stored muons), muon energy in GeV unit, experiment run time, matter density, baseline length, and target mass inside the far detector The second column gives the values of these parameters.

interested in appearance channel because disappearance channel do not provide any sensitivity on δ_{CP}. The spectrum and flavor content of neutrino beam are completely characterized by the muon decay. Therefore, with the knowledge of muon energy, we can control and obtain the corresponding event spectrum.

Obtaining event rate for neutrino appearance

Looking at the latest neutrino oscillation parameters from ref. 73, we set the oscillation parameters as shown in Table 1. The first column are the parameters used for obtaining the oscillation probability and event rates. The second column is the their central values while the third column shows the range of these parameters if marginalized. Luckily, we have here both muon and its CP-conjugated beams so that we can run both in the neutrino and antineutrino mode simultaneously. The symmetric operation of both beams leads to the cancellation or drastic reduction of many errors. Table 2 lists characteristic parameters for our simulation. Using available information from refs. 38,44,53, we can estimate the total numbers of actively decaying muons that can be stored for neutrino production is up to 10^{20}–10^{21} order of magnitude. It is worth to mention that the total events for antineutrino production is visibly smaller than that of the neutrino at the detector side because of the differences between their cross sections. Thus, we have to set a higher muon number for antineutrino mode or run a longer time for antineutrino mode. Based on the estimation method applied in GLoBES, the number of events in the ith energy for the transition from flavor $\alpha \to \beta$ are given by

$$N_i = \frac{N}{L^2}\int_0^{E_{max}} dE \int_{E_r^{min}}^{E_r^{max}} dE_r \phi(E)\sigma_{\nu_\beta} R(E, E_r) P_{\alpha\beta}(E)\epsilon(E_r), \qquad (11)$$

where N is the normalization factor proportional to run time and nuclear numbers in the target detector, L is the length of the baseline, $\phi(E)$ is the neutrino flux, ν_β is the neutrino interaction cross section, $\epsilon(E_r)$ and $R(E, E_r)$ are the efficiency and the energy resolution function of the detector. The quantities E and E_r are the true and reconstructed energies, respectively. For the detector properties, we utilize the energy resolutions and the detector efficiency provided by DUNE collaboration published on their GLoBESsimulation[34] in the case of electron and muon neutrino appearance rates. For tau neutrino event rates, we use a built-in controllable energy resolution function based on a Gaussian distribution as given

$$R^\alpha(E, E^r) = \frac{1}{\sigma(E)\sqrt{2\pi}} e^{-\frac{(E-E^r)^2}{\sigma^2(E)}}, \qquad (12)$$

where $sigma = \alpha E + \beta\sqrt{E} + \gamma$, which is taken to be $0.15E$.

Definition and minimization

χ^2 significance analysis is performed by comparing the simulated true event rates from the present best fit[74] with the events generated by the test values which is to be excluded. During the sensitivity calculation, only the solar parameters are allowed to vary while other parameter are kept fixed and constrained by Gaussian priors with 1σ standard error. The prior functions are defined as

$$\chi^2_{\text{prior}} = \left(\frac{p - p_0}{\sigma_p}\right)^2, \qquad (13)$$

where p is the oscillation parameter, p_0 is the central or true value of the prior measured by the present experiment with absolute input error σ_p. In our analysis, we apply an uncertainty of 2.5% for matter density. We construct the below χ^2 function

$$\chi^2 = \frac{\left(N(\delta_{CP}^{true}) - \overline{N}(\delta_{CP}^{true})\right)^2}{(N + \overline{N})(\delta_{CP} = 0, \pi)}. \qquad (14)$$

Here, N and $\overline{N}$ represent event rates for neutrino and antineutrino appearance.

Data availability

All the data presented with the corresponding plots in this paper are available from the corresponding author upon a reasonable request.

Received: 8 February 2023; Accepted: 17 April 2024;
Published online: 29 April 2024

References

1. Bilenky, S. M., Giunti, C. & Grimus, W. Phenomenology of neutrino oscillations. *Prog. Part. Nucl. Phys.* **43**, 1–86 (1999).
2. Nunokawa, H., Parke, S. J. & Valle, J. W. F. CP violation and neutrino oscillations. *Prog. Part. Nucl. Phys.* **60**, 338–402 (2008).
3. Blennow, M. & Smirnov, A. Y. Neutrino propagation in matter. *Adv. High Energy Phys.* **2013**, 972485 (2013).
4. Mikheyev, S. P. & Smirnov, A. Y. Resonance amplification of oscillations in matter and spectroscopy of solar neutrinos. *Sov. J. Nucl. Phys.* **42**, 913–917 (1985).
5. Bethe, H. A. A possible explanation of the solar neutrino puzzle. *Phys. Rev. Lett.* **56**, 1305 (1986).
6. Haxton, W. C., Hamish Robertson, R. G. & Serenelli, A. M. Solar neutrinos: status and prospects. *Ann. Rev. Astron. Astrophys.* **51**, 21–61 (2013).
7. Maltoni, M. & Smirnov, A. Y. Solar neutrinos and neutrino physics. *Eur. Phys. J. A* **52**, 87 (2016).
8. Fogli, G. L., Lisi, E., Marrone, A. & Montanino, D. Status of atmospheric nu(mu) — > nu(tau) oscillations and decoherence after the first K2K spectral data. *Phys. Rev. D* **67**, 093006 (2003).
9. Vergados, J. D., Ejiri, H. & Simkovic, F. Theory of neutrinoless double beta decay. *Rept. Prog. Phys.* **75**, 106301 (2012).

10. Maki, Z., Nakagawa, M. & Sakata, S. Remarks on the unified model of elementary particles. *Prog. Theor. Phys.* **28**, 870–880 (1962).
11. Pontecorvo, B. Neutrino experiments and the problem of conservation of leptonic charge. *Zh. Eksp. Teor. Fiz.* **53**, 1717–1725 (1967).
12. An, F. P. et al. Precision measurement of reactor antineutrino oscillation at kilometer-scale baselines by Daya Bay. *Phys. Rev. Lett.* **130**, 161802 (2023).
13. Adamson, P. et al. Measurement of the neutrino mixing angle θ_{23} in NOvA. *Phys. Rev. Lett.* **118**, 151802 (2017).
14. Abe, K. et al. Search for CP violation in neutrino and antineutrino oscillations by the T2K Experiment with 2.2×10^{21} protons on target. *Phys. Rev. Lett.* **121**, 171802 (2018).
15. Abe, K. et al. Atmospheric neutrino oscillation analysis with external constraints in Super-Kamiokande I-IV. *Phys. Rev. D* **97**, 072001 (2018).
16. Acero, M. A. et al. First measurement of neutrino oscillation parameters using neutrinos and antineutrinos by NOvA. *Phys. Rev. Lett.* **123**, 151803 (2019).
17. Fukugita, M. & Yanagida, T. Baryogenesis without grand unification. *Phys. Lett. B* **174**, 45–47 (1986).
18. Abe, K. et al. Constraint on the matter–antimatter symmetry-violating phase in neutrino oscillations. *Nature* **580**, 339–344 (2020) ; erratum: **583**, E16 (2020).
19. Abe, K. et al. Improved constraints on neutrino mixing from the T2K experiment with 3.13×10^{21} protons on target. *Phys. Rev. D* **103**, 112008 (2021).
20. Abe, K. et al. Measurements of neutrino oscillation parameters from the T2K experiment using 3.6×10^{21} protons on target. *Eur. Phys. J. C* **83**, 782 (2023).
21. Walsh, J. G. CP-violation search with T2K data. In *20th Conference on Flavor Physics and CP Violation*. https://arxiv.org/abs/2208.01164 (2022).
22. Acero, M. A. et al. Improved measurement of neutrino oscillation parameters by the NOvA experiment. *Phys. Rev. D* **106**, 032004 (2022).
23. Abe, K. et al. Hyper-Kamiokande design report. Preprint at https://arxiv.org/abs/1805.04163 (2018).
24. Abazajian, K. N. et al. Light sterile neutrinos: a white paper. Preprint at https://arxiv.org/abs/1204.5379 (2012).
25. Palazzo, A. Phenomenology of light sterile neutrinos: a brief review. *Mod. Phys. Lett. A* **28**, 1330004 (2013).
26. Giunti, C. & Lasserre, T. eV-scale sterile neutrinos. *Ann. Rev. Nucl. Part. Sci.* **69**, 163–190 (2019).
27. Kopp, J., Machado, P. A. N., Maltoni, M. & Schwetz, T. Sterile neutrino oscillations: the global picture. *JHEP* **05**, 050 (2013).
28. Ohlsson, T. Status of non-standard neutrino interactions. *Rept. Prog. Phys.* **76**, 044201 (2013).
29. Farzan, Y. & Tortola, M. Neutrino oscillations and non-standard interactions. *Front. Phys.* **6**, 10 (2018).
30. Acciarri, R. et al. Long-Baseline Neutrino Facility (LBNF) and Deep Underground Neutrino Experiment (DUNE): Conceptual Design Report, Volume 2: The Physics Program for DUNE at LBNF. Preprint at https://arxiv.org/abs/1512.06148 (2015).
31. Abi, B. et al. Deep Underground Neutrino Experiment (DUNE), Far Detector Technical Design Report, Volume III: DUNE Far Detector Technical Coordination. *JINST* **15**, T08009 (2020).
32. Abi, B. et al. Deep Underground Neutrino Experiment (DUNE), Far Detector Technical Design Report, Volume II: DUNE Physics. Preprint at https://arxiv.org/abs/2002.03005 (2020).
33. Abi, B. et al. Deep Underground Neutrino Experiment (DUNE), Far Detector Technical Design Report, Volume IV: Far Detector Single-phase Technology. *JINST* **15**, T08010 (2020).
34. Abi, B. et al. Experiment Simulation Configurations Approximating DUNE TDR. Preprint at https://arxiv.org/abs/2103.04797 (2021).
35. Abi, B. et al. Long-baseline neutrino oscillation physics potential of the DUNE experiment. *Eur. Phys. J. C* **80**, 978 (2020).
36. Abi, B. et al. Deep Underground Neutrino Experiment (DUNE), Far Detector Technical Design Report, Volume I Introduction to DUNE. *JINST* **15**, T08008 (2020).
37. Lu, M., Li, Q., You, Z. & Zhang, C. Richness out of smallness: a possible staged blueprint on future colliders. Preprint at https://arxiv.org/abs/2210.06690 (2022).
38. Antonelli, M., Boscolo, M., Di Nardo, R. & Raimondi, P. Novel proposal for a low emittance muon beam using positron beam on target. *Nucl. Instrum. Meth. A* **807**, 101–107 (2016).
39. Alesini, D. et al. Positron driven muon source for a muon collider. Preprint at https://arxiv.org/abs/1905.05747 (2019).
40. Tang, J., Vihonen, S. & Xu, Y. Precision measurements and tau neutrino physics in a future accelerator neutrino experiment. *Commun. Theor. Phys.* **74**, 035201 (2022).
41. Burguet-Castell, J., Gavela, M. B., Gomez-Cadenas, J. J., Hernandez, P. & Mena, O. On the measurement of leptonic CP violation. *Nucl. Phys. B* **608**, 301–318 (2001).
42. Cao, J. et al. Muon-decay medium-baseline neutrino beam facility. *Phys. Rev. ST Accel. Beams* **17**, 090101 (2014).
43. Jindariani, S. et al. Promising Technologies and R&D Directions for the Future Muon Collider Detectors. Preprint at https://arxiv.org/abs/2203.07224 (2022).
44. de Blas, J. et al. The physics case of a 3 TeV muon collider stage. Preprint at https://arxiv.org/abs/2203.07261 (2022).
45. Wolfenstein, L. Neutrino oscillations in matter. *Phys. Rev. D* **17**, 2369–2374 (1978).
46. Huber, P., Lindner, M. & Winter, W. Simulation of long-baseline neutrino oscillation experiments with GLoBES (General Long Baseline Experiment Simulator). *Comput. Phys. Commun.* **167**, 195 (2005).
47. Huber, P., Kopp, J., Lindner, M., Rolinec, M. & Winter, W. New features in the simulation of neutrino oscillation experiments with GLoBES 3.0: General Long Baseline Experiment Simulator. *Comput. Phys. Commun.* **177**, 432–438 (2007).
48. Jarlskog, C. Commutator of the quark mass matrices in the standard electroweak model and a measure of maximal CP nonconservation. *Phys. Rev. Lett.* **55**, 1039 (1985).
49. Zyla, P. A. et al. Review of particle physics. *PTEP* **2020**, 083C01 (2020).
50. Agarwalla, S. K., Kao, Y. & Takeuchi, T. Analytical approximation of the neutrino oscillation matter effects at large θ_{13}. *JHEP* **04**, 047 (2014).
51. Sharma, K. & Patra, S. Impact of CP violation searches at MOMENT experiment with sterile neutrino. *JHEP* **08**, 100 (2023).
52. Akhmedov, E. K., Johansson, R., Lindner, M., Ohlsson, T. & Schwetz, T. Series expansions for three flavor neutrino oscillation probabilities in matter. *JHEP* **04**, 078 (2004).
53. Stratakis, D. et al. A Muon Collider Facility for Physics Discovery. Preprint at https://arxiv.org/abs/2203.08033 (2022).
54. Quigg, C. Physics with a millimole of muons. *AIP Conf. Proc.* **435**, 242–257 (1998).
55. Formaggio, J. A. & Zeller, G. P. From eV to EeV: neutrino cross sections across energy scales. *Rev. Mod. Phys.* **84**, 1307–1341 (2012).
56. De Gouvêa, A., Kelly, K. J., Stenico, G. V. & Pasquini, P. Physics with beam tau-neutrino appearance at DUNE. *Phys. Rev. D* **100**, 016004 (2019).
57. Ahdida, C. et al. The SHiP experiment at the proposed CERN SPS Beam Dump Facility. *Eur. Phys. J. C* **82**, 486 (2022).
58. Branco, G. C. et al. Theory and phenomenology of two-Higgs-doublet models. *Phys. Rept.* **516**, 1–102 (2012).
59. de Medeiros Varzielas, I. & Talbert, J. Simplified models of flavourful leptoquarks. *Eur. Phys. J. C* **79**, 536 (2019).
60. Qian, S. et al. The physics case for neutrino neutrino collisions. *J. Phys. G: Nucl. Part. Phys* **51**, 045005 (2024).

61. Andreopoulos, C. et al. The GENIE Neutrino Monte Carlo Generator. *Nucl. Instrum. Meth. A* **614**, 87–104 (2010).
62. Andreopoulos, C. et al. The GENIE Neutrino Monte Carlo Generator: physics and user manual. Preprint at https://arxiv.org/abs/1510.05494 (2015).
63. Tena-Vidal, J. et al. Neutrino-nucleon cross-section model tuning in GENIE v3. *Phys. Rev. D* **104**, 072009 (2021).
64. Tang, J., Vihonen, S. & Wang, T.-C. Precision measurements on δ_{CP} in MOMENT. *JHEP* **12**, 130 (2019).
65. Schael, S. et al. Precision electroweak measurements on the *Z* resonance. *Phys. Rept.* **427**, 257–454 (2006).
66. Abdurashitov, J. N. et al. Measurement of the response of a Ga solar neutrino experiment to neutrinos from an Ar-37 source. *Phys. Rev. C* **73**, 045805 (2006).
67. Kaether, F., Hampel, W., Heusser, G., Kiko, J. & Kirsten, T. Reanalysis of the GALLEX solar neutrino flux and source experiments. *Phys. Lett. B* **685**, 47–54 (2010).
68. Athanassopoulos, C. et al. Evidence for anti-muon-neutrino — > anti-electron-neutrino oscillations from the LSND experiment at LAMPF. *Phys. Rev. Lett.* **77**, 3082–3085 (1996).
69. Aguilar-Arevalo, A. A. et al. A search for electron neutrino appearance at the $\Delta m^2 \sim 1eV^2$ scale. *Phys. Rev. Lett.* **98**, 231801 (2007).
70. Aguilar-Arevalo, A. A. et al. MiniBooNE and MicroBooNE combined fit a 3+1 sterile neutrino scenario. *Phys. Rev. Lett.* **129**, 201801 (2022).
71. Reyimuaji, Y. & Liu, C. Prospects of light sterile neutrino searches in long-baseline neutrino oscillations. *JHEP* **06**, 094 (2020).
72. de Gouvêa, A., Jusino Sánchez, G. & Kelly, K. J. Very light sterile neutrinos at NOvA and T2K. *Phys. Rev. D* **106**, 055025 (2022).
73. Workman, R. L. et al. Review of particle physics. *PTEP* **2022**, 083C01 (2022).
74. Esteban, I., Gonzalez-Garcia, M. C., Maltoni, M., Schwetz, T. & Zhou, A. The fate of hints: updated global analysis of three-flavor neutrino oscillations. *JHEP* **09**, 178 (2020).

Acknowledgements

This work is supported in part by the National Natural Science Foundation of China under Grants Nos. 12150005, 12075004, and 12061141002, by MOST under grant No. 2018YFA0403900. The authors would like to thank Joachim Kopp, Haixing Lin and Jian Tang for useful discussions.

Author contributions

Qiang Li provided the main experimental idea, and Alim Ruzi conducted the simulations and drafted the article. Tianyi Yang provided the results displayed in Fig. 4. Dawei Fu, Sitian Qian, and Leyun Gao were responsible for revising the whole article.

Competing interests

The authors declare no competing interests.

Additional information

Supplementary information The online version contains supplementary material available at https://doi.org/10.1038/s42005-024-01633-6.

Correspondence and requests for materials should be addressed to Alim Ruzi or Qiang Li.

Peer review information *Communications Physics* thanks the anonymous reviewers for their contribution to the peer review of this work. A peer review file is available.